The Astrophysical Journal Letters, 967:L45 (8pp), 2024 June 1 https://doi.org/10.3847/2041-8213/ad4a7a
© 2024. The Author(s). Published by the American Astronomical Society.
OPEN ACCESS

Light Curves of the Explosion of ONe White Dwarf + CO White Dwarf Merger Remnant and Type Icn Supernovae

Chengyuan Wu[1,2], Shuai Zha[1,2], Yongzhi Cai[1,2], Zhengyang Zhang[1,2,3], Yi Yang[4], Danfeng Xiang[4], Weili Lin[4], Xiaofeng Wang[4], and Bo Wang[1,2]
[1] Yunnan Observatories, Chinese Academy of Sciences, Kunming 650216, People's Republic of China; wuchengyuan@ynao.ac.cn
[2] International Centre of Supernovae, Yunnan Key Laboratory, Kunming, 650216, People's Republic of China
[3] University of Chinese Academy of Sciences, Beijing 100049, People's Republic of China
[4] Physics Department and Tsinghua Center for Astrophysics, Tsinghua University, Beijing, 100084, People's Republic of China
Received 2024 February 6; revised 2024 May 8; accepted 2024 May 10; published 2024 May 31

Abstract

Type Icn supernovae (SNe Icn) are a newly detected, rare subtype of interacting stripped-envelope supernovae that show narrow P Cygni lines of highly ionized carbon, oxygen, and neon in their early spectra due to the interactions of the SNe ejecta with dense hydrogen- and helium-deficient circumstellar material (CSM). It has been suggested that SNe Icn may have multiple progenitor channels, such as the explosion of carbon-rich Wolf–Rayet stars or the explosion of stripped-envelope SNe, which undergo binary interactions. Among the SNe Icn, SN 2019jc shows unique properties, and previous work inferred that it may stem from the ultrastripped supernova, but other possibilities still exist. In this work, we aim to simulate the light curves from the explosions of oxygen-neon and carbon-oxygen double white dwarf (WD) merger remnants and to further investigate whether the corresponding explosions can appear as some particular SNe Icn. We generate the light curves from the explosive remnants and analyze the influence of different parameters on the light curves, such as the ejecta mass, explosion energy, mass of ^{56}Ni, and CSM properties. Comparing our results with some SNe Icn, we found that the light curves from the explosions of double WD merger remnants can explain the observable properties of SN 2019jc, from which we infer that this special SN Icn may have a different progenitor. Our results indicate that double WD merger may be an alternative model in producing at least one of the SNe Icn.

Unified Astronomy Thesaurus concepts: White dwarf stars (1799); Stellar mergers (2157); Supernovae (1668); Core-collapse supernovae (304)

1. Introduction

It is widely believed that massive stars with initial masses greater than 8−12 $M_{\odot}$ will end their lives exploding as core-collapse supernovae (CCSNe), which can be classified into different types from their spectral properties (e.g., Filippenko 1997; Gal-Yam 2017). CCSNe that show hydrogen (H) lines in their spectra are classified as Type II SNe, while those that show a complete absence of H features in their spectra or show evidence of H only at early times are called H-poor or stripped-envelope SNe (SESNe), including Types Ib, Ic, and IIb SNe. Some CCSNe that show evidence for interactions between the SNe ejecta and circumstellar material (CSM) are named as interacting SNe. The interacting SNe that exhibit bright and narrow Balmer lines of H in their spectra are classified as Type IIn SNe, while the events that display narrow lines of helium (He) in their spectra without H, indicating the presence of a H-poor but He-rich CSM around the exploding stars, are named Type Ibn SNe. Recently, an even more extreme subtype of interacting SESNe, named Type Icn supernovae (SNe Icn), has been discovered (e.g., Fraser et al. 2021; Gal-Yam et al. 2022). The early-time spectra of SNe Icn are blue with narrow P Cygni lines of highly ionized carbon (C), oxygen (O), and neon (Ne) instead of He. These SNe show rapid photometric evolution with a high peak brightness. After the maximum light, as the SN ejecta become optically thin, their spectra appear more similar to normal SNe Ibc or SNe Ibn but still remain different (e.g., Gal-Yam et al. 2022; Perley et al. 2022; Davis et al. 2023).

Up to now, only five SNe Icn have been reported, i.e., SN 2019hgp, SN 2019jc, SN 2021csp, SN 2021ckj, and SN 2022ann (e.g., Fraser et al. 2021; Perley et al. 2022; Gal-Yam et al. 2022; Pellegrino et al. 2022; Nagao et al. 2023; Davis et al. 2023). The origins of SNe Icn are still under debate. Gal-Yam et al. (2022) proposed a Wolf–Rayet (WR) star to be the progenitor of SN 2019hgp based on its observational properties and suggested a possibility that the differences between SNe Ibn and SNe Icn arise from their different types of WR star progenitors, i.e., He- and nitrogen (N)-rich WN stars for SNe Ibn and C-rich WC stars for SNe Icn. Perley et al. (2022) suggested that a WR star directly collapsing to a black hole can launch a subrelativistic jet, and the jet's interaction with the dense CSM may explain the observational properties of SN 2021csp. Nagao et al. (2023) suggested that SN 2021csp and SN 2021ckj may have aspherical ejecta and spherical CSM, and the different observational properties between these two SNe arise from the viewing-angle effects (see also Fraser et al. 2021), i.e., the SN 2021ckj is observed from a direction close to the jet pole, while SN 2021csp is observed from an off-axis direction. Davis et al. (2023) found that the CSM of SN 2022ann only has a velocity of about 800 km s^{-1}, which is inconsistent with the typical velocity of WR star winds. Moreover, the host galaxy of SN 2022ann is a low-mass dwarf galaxy with low star formation rate and low average metallicity, suggesting that the progenitor of SN 2022ann has low metallicity. This implies that it is difficult to fully strip the

Original content from this work may be used under the terms of the Creative Commons Attribution 4.0 licence. Any further distribution of this work must maintain attribution to the author(s) and the title of the work, journal citation and DOI.

H/He envelope from its progenitor through stellar wind (a massive WR star may not be the progenitor of SN 2022ann). Instead, they suggested a binary-stripped progenitor for SN 2022ann, rather than a single, massive WR progenitor. Pellegrino et al. (2022) analyzed a sample of four SNe Icn, including SN 2019hgp, SN 2019jc, SN 2021ckj, and SN 2021csp. They found that SN 2019jc shows different features compared with other SNe Icn in the following aspects: first, this SN is unique in having a light curve that is both faster evolving and fainter than those of other SNe Icn; second, SN 2019jc is located at the outer edge of its host galaxy, where the star formation rate density is low. Based on a circumstellar interaction model, Pellegrino et al. (2022) fitted the bolometric light curves of these four SNe Icn and found that SN 2019jc has low explosion energy and low ejecta mass, suggesting a low-mass, ultrastripped SN as its progenitor. However, for other SNe Icn, the WR star progenitors or binary systems may better explain their observational properties.

Recently, Wu et al. (2023) investigated the evolution of the postmerger remnants from the coalescence of ONe and CO WD pairs. They found that the merger remnants could evolve to H-/He-deficient giant-like stars due to shell-carbon burning. The merger remnants with masses greater than 1.95 $M_{\odot}$ can explode as electron-capture SNe (ECSNe) and can produce CO-rich CSM resulting from the stellar wind during their giant phases. The interactions between the SNe ejecta and CSM may produce narrow C, O, and Ne emission lines similar to SNe Icn, making the double WD merger able to be a potential channel in producing SNe Icn even though some of the SNe Icn observed at early times show He emission lines (for example, the spectrum of SN 2019jc at maximum light shows a He II λ4686 feature), suggesting that the CSM surrounding SNe Icn may not be fully devoid of He. Note that there could exist a He surface layer on the CO WD, which causes the merger remnant involving at least one CO WD to contain some amount of He (e.g., Dan et al. 2014; Schwab 2021; Wu et al. 2023). The subsequent evolution of such a merger remnant may produce CSM that is dominated by C, O, and Ne but not completely devoid of He through stellar wind, which means that it is possible to detect He emission lines from the early-time spectra of some SNe Icn if these SNe stem from the double WD merger channel. Since the optical light curves from the explosions of the massive double WD merger remnants have not been well studied, in this work, we are going to simulate the light curves from the explosions of merger remnants and then compare them with some SNe Icn.

The rest of the Letter is organized as follows: In Section 2, we introduce the method in generating the light curves of exploding double WD merger remnants. In Section 3, we analyze how different sets of parameters influence the light curves. In Section 4, we compare our simulated light curves to some SNe Icn and discuss whether our model can explain SNe Icn. Finally, the summary is provided in Section 5.

2. Model Setups

As investigated by previous works, ONe+CO WD merger remnants with masses greater than 1.95 $M_{\odot}$ will end their lives as ECSNe (e.g., Wu et al. 2023). The collapse of the ONe core releases a large amount of gravitational potential energy, which can be transformed to thermal and kinetic energy to power a bright transient. In order to calculate the light curves from the explosions of double WD merger remnants, we take the stellar structures at their final evolutionary stages (just prior to the core collapse) from Wu et al. (2023) as our initial models. Then we evolve the models from a few seconds after the central explosions triggered by core collapse to a time just before the outgoing shocks reach the stellar surface by employing the Modules for Experiments in Stellar Astrophysics (MESA, version 12778; e.g., Paxton et al. 2011, 2013, 2015, 2018, 2019). Subsequently, we use radiation hydrodynamics code STELLA (e.g., Blinnikov & Bartunov 1993; Blinnikov & Panov 1996; Blinnikov et al. 1998, 2000, 2006; Blinnikov & Tolstov 2011) to evolve the models from the shock breakout to several tens of days to generate the light curves.

In detail, our approach is as follows. First, we consider the most massive merger remnant described in Wu et al. (2023) as our initial model (i.e., 2.25 $M_{\odot}$, resulting from a 1.20 $M_{\odot}$ ONe WD merger with a 1.05 $M_{\odot}$ CO WD). The central core temperature of this model achieves $\log(T_c/\mathrm{K}) = 9.3$ when core collapse occurs, and the radius of the remnant is about 377 $R_{\odot}$ at that moment. To investigate the effect of ejecta mass on the light curves, we remove different central sections from the initial model. We assume three mass cuts, i.e., 1.42 $M_{\odot}$ (just above the CO-burning layer), 1.65 $M_{\odot}$ and 1.89 $M_{\odot}$, corresponding to the ejecta masses equal to 0.83 $M_{\odot}$, 0.60 $M_{\odot}$, and 0.36 $M_{\odot}$, respectively. The mass profile and density structure of the initial model as well as the positions of different mass cuts are shown in panels (a) and (b) of Figure 1.

Second, we put the structures above the mass cuts into the explosion calculations. According to the numerical explosion simulations, the explosion energy of ECSNe is in an order of magnitude of 10^{50} erg (e.g., Kitaura et al. 2006; Moriya & Eldridge 2016; Zha et al. 2022). To explore the influence of explosion energy on the light curves, we inject different energies (i.e., 0.05 B, 0.10 B, and 0.20 B; 1 B $\equiv 10^{51}$ erg) into a thin layer of about 0.01 $M_{\odot}$ at the inner boundary of the remaining envelope within 5 ms.

Third, we calculate the shock-propagating process from the innermost shell of the envelope toward the surface. Since it is important to have enough unshocked material for the STELLA code to calculate the light curves, we stop our MESA simulations once there is $\sim$0.05 $M_{\odot}$ unshocked material remaining between the shock and the surface. During the shock-propagating process, we ignore all the nuclear reactions to keep the elemental abundance distributions in the envelope unchanged. Note that ^{56}Ni can be generated by the intense nuclear burning behind the shock near the core–envelope boundary just after core collapse, and numerical simulations indicated that the mass of ^{56}Ni produced in ECSNe and accretion-induced-collapse events would be in the order of magnitude of 10^{-3}–10^{-4} $M_{\odot}$ (e.g., Dessart et al. 2006; Moriya & Eldridge 2016). To explore how the mass of ^{56}Ni affects the light curves, we artificially add different masses of ^{56}Ni (i.e., 0.0001$M_{\odot}$, 0.001 $M_{\odot}$, and 0.01 $M_{\odot}$) in the envelope. This goal is achieved by reducing the mass of ^{16}O and replacing with ^{56}Ni. Besides, previous works suggested that the ^{56}Ni mixing process may influence the sharpness of light curves (e.g., Moriya et al. 2020). In our simulations, we considered two different degrees of mixing. In the "full mixing" model, ^{56}Ni is uniformly mixed in the entire ejecta, while in the "half mixing" model, the outer edge of the layer where ^{56}Ni is mixed is in the center of the envelope. The elemental abundance distribution profile of the ejecta with 0.001 $M_{\odot}$ of ^{56}Ni is shown in panel (c) of Figure 1.

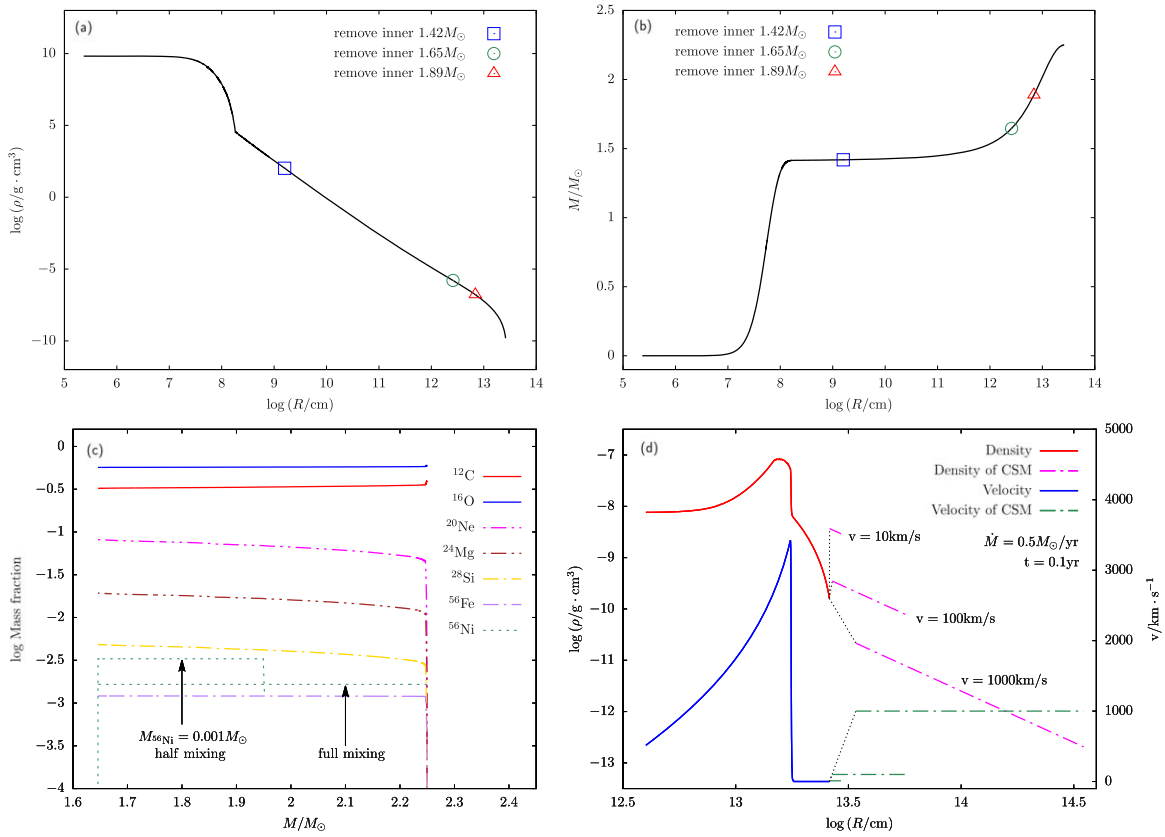


Figure 1. Properties of the merger remnant before light-curve calculations. Panels (a) and (b) represent the density profile and the enclosed mass as the function of radius of the merger remnant before explosion. Blue squares, green circles, and red triangles represent the different mass cuts before energy injection. Panels (c) and (d) represent the elemental abundance profile and the density and velocity profiles of the 0.6 $M_\odot$ ejecta at the moment when shock wave reached the position at 0.05 $M_\odot$ beneath the surface. Panel (c) also shows the elemental abundance distribution in considering ^{56}Ni with half and full mixing. Panel (d) also shows the properties of CSM with different wind velocities (wind mass-loss rate of 0.5 $M_\odot$ yr^{-1} lasts for 0.1 yr prior to the SN explosion).

Finally, after the outer edge of the shock reaches the desired position, we save the STELLA data by adopting "stella _ num _ points=400," where 400 is a recommended value in MESA default. Note that the stellar winds of the merger remnants prior to their explosions may form CSM surround the progenitors, and the ejecta interacting with CSM could transform kinetic energy into thermal energy and thus influence the light curves. To investigate this effect, we attach the CSM on the top of the progenitors and use "stella _ nz _ extra=40" to save the data of CSM properties. We consider the wind-like CSM. Based on the evolutionary results from the previous work (e.g., Wu et al. 2023), the merger remnants could have enormous wind mass-loss rates just prior to the SN explosions (the time intervals between the significant wind mass-loss processes and the SN explosions are within tens of days to several years, which are influenced by the total masses of the merger remnants and the wind mass-loss prescriptions), which means that the outer radii of the CSM surrounding the SNe are not too large. For the wind-like CSM, the wind density parameter (w) is very useful in directly estimating the density of the CSM ($\rho_{\rm CSM}$), i.e.,

$$w = \frac{\dot{M}}{v_{\rm wind}}, \quad (1)$$

and

$$\rho_{\rm CSM}(\mathrm{r}) = \frac{w}{4\pi r^{-2}}, \quad (2)$$

where, $\dot{M}$ is the mass-loss rate of the progenitors, $v_{\rm wind}$ is the velocity of the stellar wind, and r is the radius of the CSM (e.g., Blinnikov 2017). Since the wind velocities and mass-loss rates of such H-/He-deficient giants are not well constrained from the observations, in the current work, we consider various wind velocities ($v = 10\,\mathrm{km\,s^{-1}}$, $100\,\mathrm{km\,s^{-1}}$, and $1000\,\mathrm{km\,s^{-1}}$, corresponding to the typical wind velocities of red giant branch (RGB)/asymptotic giant branch (AGB) stars, yellow supergiants, and WR stars, respectively; e.g., Smith 2017), wind density parameters ($3.15\times10^{17} - 3.15\times10^{19}\,\mathrm{g\,cm^{-1}}$, depending on the evolution of the progenitor stars under different wind mass-loss parameters), and total masses of CSM ($M_{\rm CSM} = 0.05$ and $0.25\ M_\odot$). The density and velocity profiles of the remnants and CSM (an example that we assume the enormous wind mass-loss rate, i.e., 0.5 $M_\odot$ yr^{-1}, occurs 0.1 yr prior to the SN explosion) are provided in panel (d) of Figure 1.

3. Bolometric Light Curves

We use the multigroup radiation hydrodynamics code STELLA to follow the evolution of the explosion models described above through shock breakout to 70 days after explosion. STELLA is able to simulate SN evolution at early times and can also solve the shock breakout and interaction between ejecta and CSM. In the calculation, SN explosion is regarded as a thermal bomb located at the inner boundary of the ejecta. STELLA solves the radiative transfer equations in the intensity momentum approximation in each frequency bin. We use 40 frequency bins, which are enough to generate bolometric light curves. The opacity is computed based on

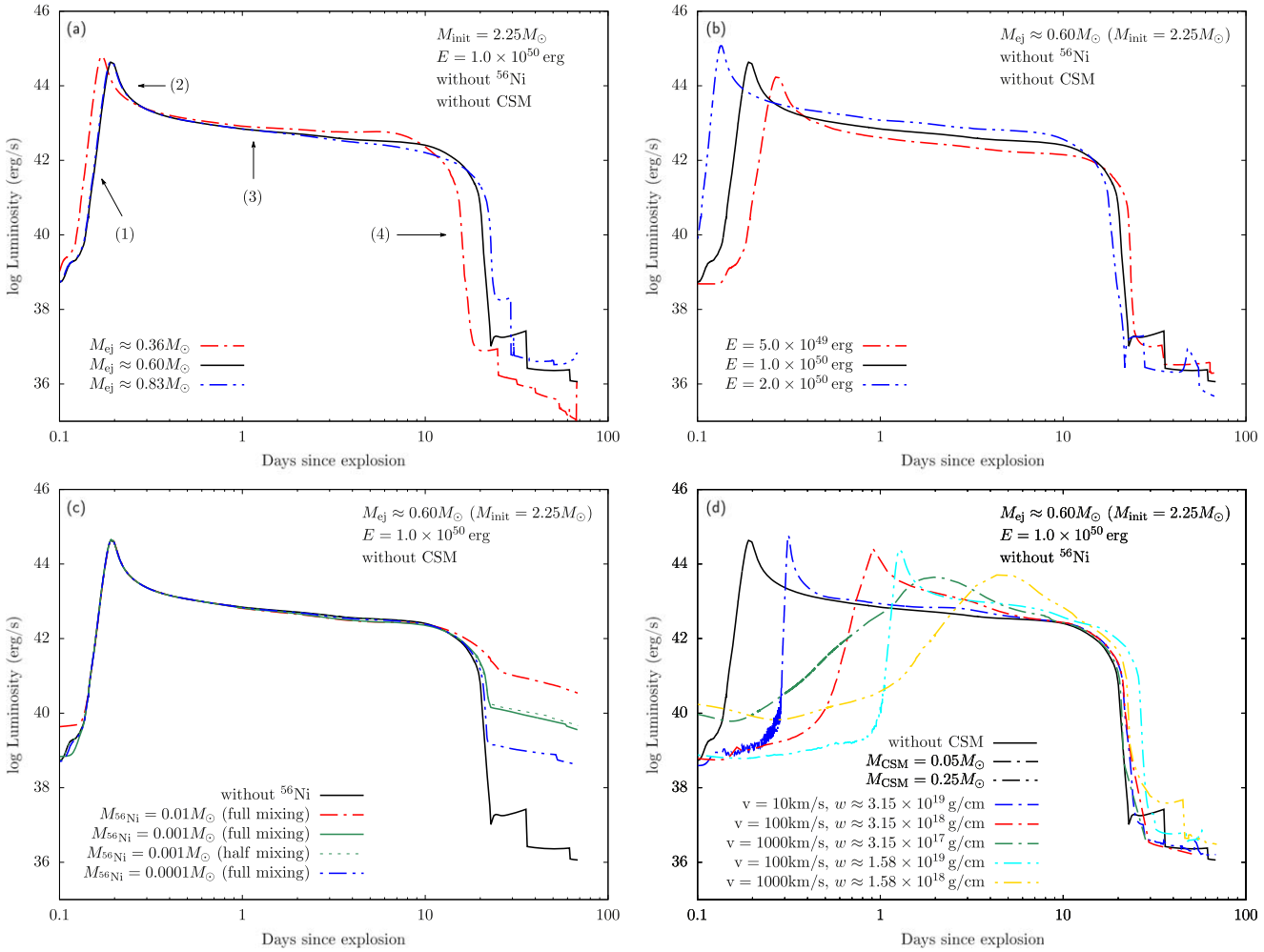


Figure 2. Light curves from the explosions of double WD merger remnants with different initial parameters, demonstrating how the parameters alter the light curves. Panel (a): the effect of ejecta mass ($M_{\rm ej}$). Panel (b): the effect of explosion energy (E). Panel (c): the effect of ^{56}Ni mass ($M_{^{56}\rm Ni}$) and mixing. Panel (d): the effect of CSM properties. Numbers (1)–(4) in panel (a) represent the four evolutionary phases mentioned in Section 3.

over 153,000 spectral lines from Kurucz & Bell (1995) and Verner et al. (1996). Some simulated outputs from our STELLA simulations are publicly available on Zenodo at doi:10.5281/zenodo.11066927.

We present the light curves from different progenitors described above (Section 2) in Figure 2, while the evolution of blackbody temperature, density, radius, velocity, and opacity of a specific model (i.e., $M_{\rm ej} = 0.60\ M_\odot$, $E = 0.1$ B, without ^{56}Ni, without CSM) are presented in Figure 3. The overall evolutionary characteristics of the luminosity are as follows (four evolutionary phases).

(1) Rapid increasing phase: at the beginning of the evolution, the ejecta is heated and ionized by the outwardly propagating explosion shock wave.
(2) Rapid declining phase: after the shock breakout, the evolution of the bolometric luminosity is powered by the diffusion of thermal energy deposited in the ejecta, and during this stage, the luminosity declines quickly.
(3) Plateau phase: as the ejecta expands and cools, the temperature of the material gradually drops below the recombination temperature and the ejecta becomes largely transparent. The composition of the ejecta in our model is mixed mainly with ^{12}C, ^{16}O, ^{20}Ne, and ^{24}Mg. For this mixture, the recombination temperature is about 6000 K. For the higher temperature ($T > 6000$ K), the opacity of the mixture is greater than about 0.04 cm^2 g^{-1}. When the temperature drops below 6000 K, oxygen recombines to neutral, and the opacity drops dramatically, which is similar to the O-Ne-Mg mixture (e.g., Kleiser & Kasen 2014). As the outer layers of the ejecta begin to recombine, a sharp ionization front develops in the ejecta. At this moment, the photosphere stays at the recombination front, and the luminosity decline rate becomes significantly smaller than before, resulting in the appearance of a plateau-like feature.
(4) Late phase: the plateau phase lasts for about 10–25 days, depending on the initial structures of the progenitors and after which the recombination wave reaches the center of the ejecta, exhausting the energy stored in the ejecta, and the light curve drops off extremely rapidly, bringing the end of the plateau phase.

The duration of the plateau phase is dominated by the dissipation rate of the energy stored in the ejecta. From Figure 2, we can see that the ejecta mass and the explosion energy can significantly effect the plateau luminosity and the duration of plateau phase (panels (a) and (b)). Under the same explosion energy, a more massive ejecta mass leads to a lower plateau luminosity. This is because when the recombination front developed in the envelope, the ejecta usually has similar

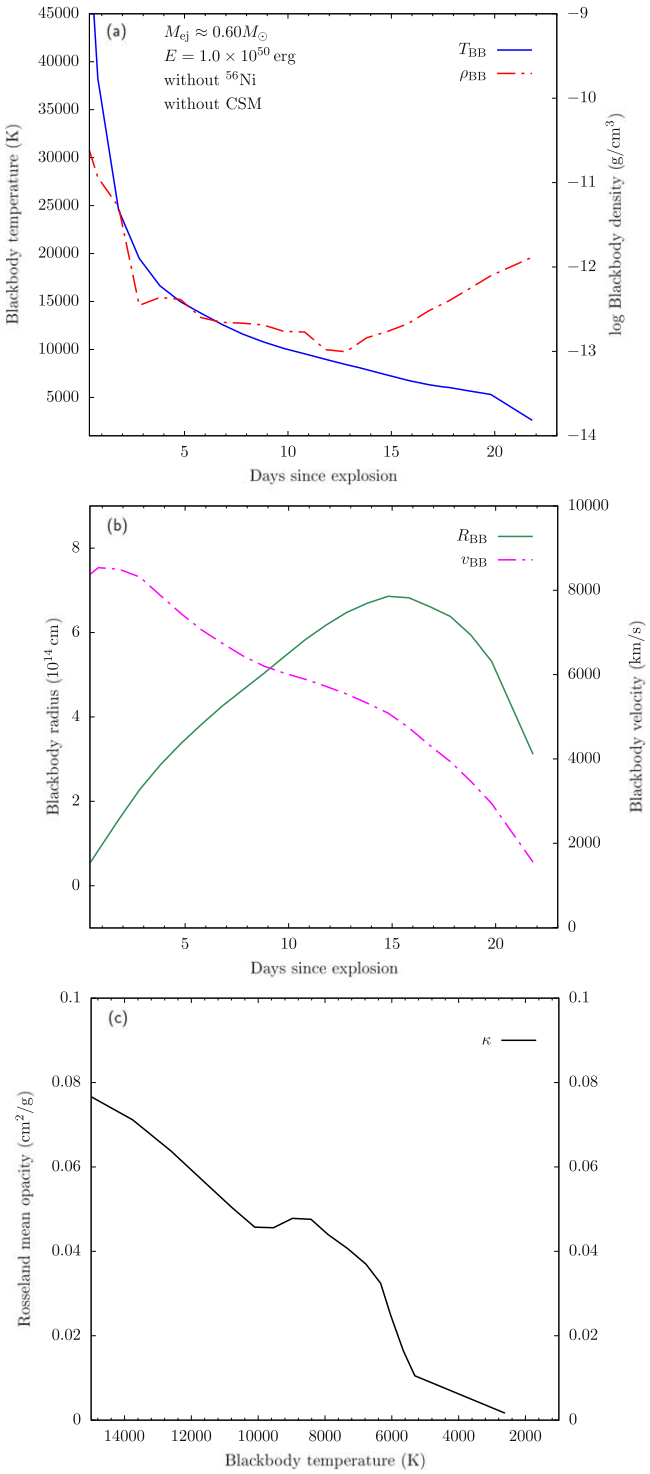


Figure 3. Additional properties of the merger remnant ($M_{ej} = 0.60\ M_\odot$, $E = 1.0 \times 10^{50}$ erg) after explosion. Panels (a) and (b): blackbody temperature, density, radius, and velocity as functions of time. Panel (c): Rosseland mean opacity at the photosphere as a function of temperature.

photosphere temperature, but a more massive ejecta has lower expansion velocity, which causes a smaller photosphere radius. In addition, a lower expansion velocity makes the energy deposited in the envelope require more time to be exhausted; hence, the plateau phase is longer for a more massive ejecta mass. The effect of explosion energy on the light curves is similar to that of the ejecta mass, i.e., a higher explosion energy leads to a more luminous but shorter plateau phase and vice versa.

After the SN explosion, the nuclear burning behind the shock wave is able to produce iron-group elements such as ^{56}Ni in the ejecta. The radioactive decay of ^{56}Ni can heat the envelope and thus increase the bolometric luminosity. In panel (c) of Figure 2, we compare the light curves of the progenitor models with different masses of ^{56}Ni. Various masses of ^{56}Ni cannot influence the light curves during the plateau phase significantly. About 15 days after explosion, the radioactive decay of isotopes gradually dominates the evolution of the luminosity, and an increase by 10 times of ^{56}Ni mass will cause an order of magnitude increase in the tail bolometric luminosity. Theoretically, if ^{56}Ni is entirely mixed in the ejecta, the heating caused by radioactive decay in the outer layers of the ejecta becomes efficient, which leads to the increase in luminosity to occur earlier than that if ^{56}Ni is only located at the inner portion of the ejecta. However, due to the low ^{56}Ni mass generated from ECSNe, the plateau luminosity is still dominated by the energy deposited in the envelope, which means that the degree of ^{56}Ni mixing may not effect the light curves significantly in the current situation.

After the merger of double WDs, the remnant can evolve to a giant phase, during which the H-/He-deficient CSM is formed due to the stellar wind. The interaction between ejecta and CSM can transform kinetic energy into thermal energy and thus alter the features of the light curves. The interacting process is mainly influenced by the properties of the CSM such as its radius and its density distribution. In panel (d) of Figure 2, we present the light curves of the explosion remnants with different CSM properties. Since the wind mass-loss rates and wind velocities of such merger remnants are not well constrained, we artificially added 0.05 $M_\odot$ or 0.25 $M_\odot$ of CSM surrounding the progenitor. The density profile of the CSM is dominated by the wind density parameters, and in these simulations, the parameter w is in the range between 3.15×10^{17} and 3.15×10^{19} g cm^{-1}, which is related to the wind mass-loss histories of the progenitors. We consider three different wind velocities, i.e., $v = 10$ km s^{-1}, $v = 100$ km s^{-1}, and $v = 1000$ km s^{-1}, corresponding to the typical wind velocity of RGB/AGB stars, yellow supergiants and WR stars, respectively (e.g., Smith 2017). From panel (d) of Figure 2, we can see that the early bolometric luminosity becomes higher when the wind density parameter of CSM is higher because of the extra radiation from CSM interaction. A longer CSM interaction resulting from the larger radius of the CSM causes the delayed appearance of peak luminosity in the light curves. Afterwards, all the light curves are restored to similar evolutionary paths, indicating the end of the CSM interaction.

4. Comparing to Observations

To date, five SNe Icn have been reported. According to the analyses from the previous works, it seems that this new type of SNe may have multiple formation channels (e.g., Gal-Yam et al. 2022; Perley et al. 2022; Pellegrino et al. 2022). In order to investigate whether any SNe Icn may have originated from the postmerger remnants resulting from the coalescence of ONe and CO WD pairs, we obtain some observational data of three SNe Icn, i.e., SN 2019hgp, SN 2019jc, and SN 2021csp from Pellegrino et al. (2022), and compare our models to the observational data. The properties of the progenitors and the CSM are based on the evolutionary results of a 2.25 $M_\odot$ double WD merger remnant provided in Wu et al. (2023). During the final evolutionary stages of the merger remnants, there exist strong wind mass-loss processes, which lead to the decrease in

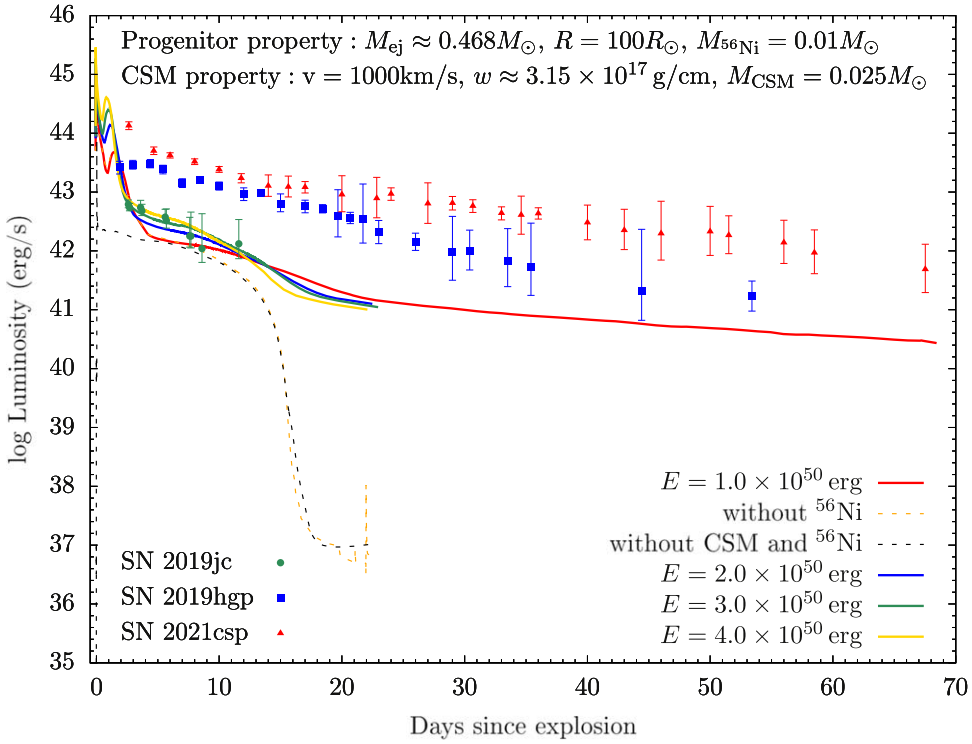


Figure 4. The comparison between light curves from the explosions of double WD merger remnants and the bolometric light curves of three SNe Icn. In the light-curve simulations, the radius of progenitor is $R = 100\ R_\odot$, the ejecta mass is $M_{ej} \approx 0.468\ M_\odot$, and the mass of nickel $M_{^{56}Ni} = 0.01 M_\odot$, fully mixed into the ejecta. For the property of CSM, the wind velocity is $v = 1000$ km s^{-1}, the wind density parameter is $w \approx 3.15 \times 10^{17}$ g cm^{-1}, and the mass of the CSM is $M_{CSM} = 0.025\ M_\odot$. Solid lines with different colors represent the light curves from our simulations with different explosive energies (the CSM interaction and radioactive decay from ^{56}Ni are considered). Dashed lines represent the simulated light curves with explosive energy $E = 0.1$ B but without considering radioactive decay from ^{56}Ni (orange dotted line) and without considering both CSM interaction and radioactive decay from ^{56}Ni (black dotted line). For some of the models, the simulations terminate at 23 days after explosions in order to save the calculation time. Green circles, blue squares, and red triangles with error bars represent the bolometric light curves of SN 2019jc, SN 2019hgp, and SN 2021csp, respectively.

the radii of the progenitors and the formation of dense CSM. However, note that it is difficult to accurately estimate the progenitor radius and the mass of the CSM because of the uncertainty in wind mass-loss rate. Hence, in our models, we assume the enormous stellar wind decreases the radius of the progenitor down to 100 $R_\odot$, making the ejecta mass equal to 0.468 $M_\odot$, and the dense CSM mass equals to 0.025 $M_\odot$. Besides, we assume that the wind velocity equals to 1000 km s^{-1}, which is consistent with the observed CSM velocity of SNe Icn. We consider different explosion energies (from $E = 1.0 \times 10^{50}$ to 4.0×10^{50} erg) and 0.01 $M_\odot$ of ^{56}Ni in the ejecta to simulate the corresponding light curves. For comparison, we also simulate the light curves with the same progenitor/CSM properties ($R = 100\ R_\odot$, $M_{ej} = 0.468\ M_\odot$ and $E = 1.0 \times 10^{50}$ erg) but without ^{56}Ni in the ejecta or even without the interaction between ejecta and CSM.

The comparison of our simulated light curves with these three SNe is presented in Figure 4, while the comparison of the evolution of blackbody temperature and radius are presented in panels (a) and (b) of Figure 5, and the multiband light curves from two of our models ($E = 2.0 \times 10^{50}$ and 4.0×10^{50} erg) are provided in panels (c) and (d) of Figure 5. The bolometric luminosities and blackbody properties of each object are estimated through the extensive multiband observations (for more detail, see Pellegrino et al. 2022). From Figure 4, we can see that the bolometric luminosities from the explosion of double WD merger remnants are significantly lower that that of SN 2019hgp and SN 2021csp. This implies that these two SNe should have more massive ejecta masses and higher explosion energies, indicating that they may be related to the explosions of massive WR stars. Interestingly, the light curves from our models with explosion energy $E = 2.0 \times 10^{50} - 4.0 \times 10^{50}$ erg provide reasonable fits to the bolometric luminosity of SN 2019jc,[5] which means that this SN may have a different progenitor from other SNe Icn. Furthermore, SN 2019jc exploded on the outskirts of the nearby spiral galaxy, where the star formation rate density is low. The low star formation rate density argues against the progenitor with high zero-age main-sequence mass. The progenitors of WDs are low-mass main-sequence stars, and the SNe from the double WD mergers could form in any position of their host galaxies, which implies that the host galaxy environment of SN 2019jc is also consistent with the double WD merger channel. However, it is still too early to conclude that SN 2019jc is related to a double WD merger. On one hand, although the luminosities of B, V, R, and I bands are consistent with SN 2019jc, the evolution of multiband light curves obtained from our models is slower than that of SN 2019jc, which is probably because of the discrepancy in the photosphere opacity resulting from the difference of ejecta compositions or the radius of the progenitor. On the other hand, SN 2019jc was not observed until approximately 3 days after

[5] Note that the progenitor/CSM properties in our models are different from the estimated values from Pellegrino et al. (2022). However, it is difficult to constrain some properties such as ejecta mass, CSM mass, and progenitor radius from the observation directly, but the CSM velocity can be inferred from the spectra. Thus, in our models, we assume the CSM velocity is 1000 km s^{-1}, which is consistent with SNe Icn, but other parameters are related to the evolution of the progenitors.

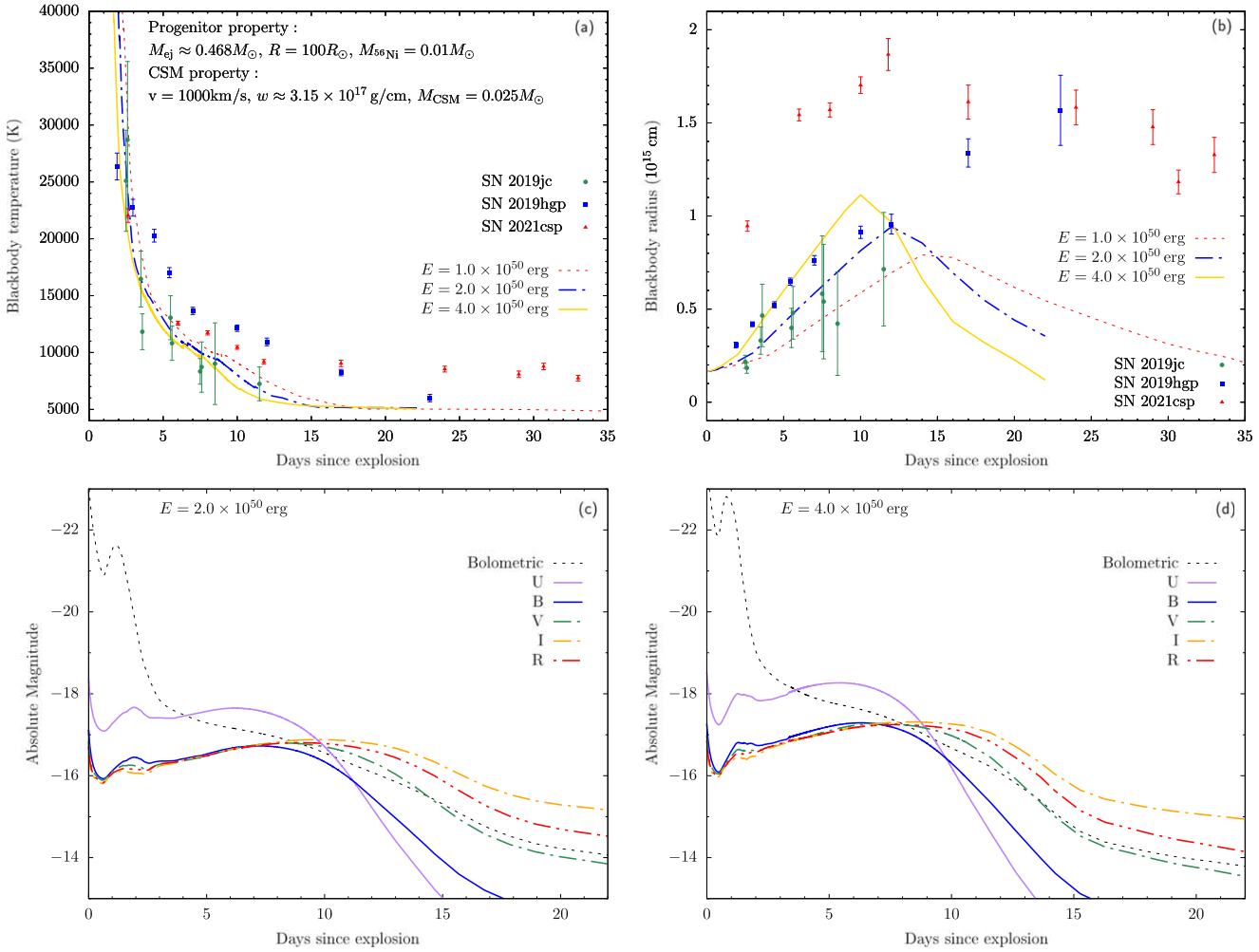


Figure 5. Panels (a) and (b): similar to Figure 4, but for the evolution of blackbody temperature (panel (a)) and blackbody radius (panel (b)). Panels (c) and (d): multiband light curves for double WD merger remnants with different explosion energies.

explosion and disappeared approximately 12 days after explosion, which cannot constrain its early-time and subsequent evolution. For the early-time evolution, our results imply that ultraviolet (UV) or X-ray radiation may have major contribution to the bolometric light curves. For the late-time evolution, the existence of ^{56}Ni in the ejecta can significantly influence the luminosity after the plateau phase. Hence, the early-time UV or X-ray observations and the late-time observational data are needed in constraining the progenitor channel of SN 2019jc. Currently, even though we cannot provide any better limitations on the origin of SN 2019jc depending on the limited data, we suggest that the explosion of a double WD merger remnant may be a new model in explaining the observational properties of SN 2019jc, but other progenitor channels such as ultrastripped SN or stripped envelope of ECSN (e.g., Tauris et al. 2013; Tauris et al. 2015; Moriya & Eldridge 2016) are still possible.

5. Summary

In this work, we simulated the light curves from the explosion of ONe+CO WD merger remnants. We found that the light curves decline quickly after the shock breakout and enter into the plateau phases resulting from the recombination of ionized carbon and oxygen. After the energy stored in the envelope is exhausted, the light curves drop off rapidly. In the simulations, we analyzed the influences of different parameters such as ejecta mass, explosion energy, ^{56}Ni mass, and different properties of CSM. The ejecta mass and explosion energy can effect the plateau bolometric luminosities and their durations. A higher explosion energy or a lower ejecta mass leads to a more luminous but shorter plateau phase and vice versa. The ^{56}Ni mass can effect the tail bolometric luminosity. An increase by 10 times of ^{56}Ni mass will cause an order of magnitude increasing in the tail bolometric luminosity. The density and the size of CSM can effect the peak luminosity due to the CSM interaction. Furthermore, we compare the simulated light curves with some SNe Icn. We found that the light curves from the explosion of a double WD merger remnant can fit the bolometric luminosity of SN 2019jc within 12 days after explosion but is significantly fainter than that of SN 2019hgp and SN 2021csp. We proposed that a double WD merger may be an alternative progenitor channel of at least one SN Icn. In order to better understand the progenitor systems of SN Icn and their explosion mechanisms, more SN Icn samples with high-quality data (such as early-time UV or X-ray observations) are needed in the future.

Acknowledgments

We thank the anonymous referee for very helpful suggestions on the manuscript. We thank Dongdong Liu, Zhenwei Li for

helpful discussion. This study is supported by the National Natural Science Foundation of China (Nos. 12225304, 12288102, 12090040/12090043, 12303054, 12393811), the National Key R&D Program of China (No. 2021YFA1600404), the Yunnan Revitalization Talent Support Program—Young Talent project, the Western Light Project of CAS (No. XBZG-ZDSYS-202117), the science research grant from the China Manned Space Project (No. CMS-CSST-2021-A12), the Frontier Scientific Research Program of Deep Space Exploration Laboratory (No. 2022-QYKYJH-ZYTS-016), the Yunnan Fundamental Research Project (Nos. 202301AU070039, 202201BC070003, 202301AU070109, 202401AU070063), and the International Centre of Supernovae, Yunnan Key Laboratory (No. 202302AN360001).

ORCID iDs

Chengyuan Wu https://orcid.org/0000-0002-2452-551X
Shuai Zha https://orcid.org/0000-0001-6773-7830
Yongzhi Cai https://orcid.org/0000-0002-7714-493X
Zhengyang Zhang https://orcid.org/0009-0006-8370-3108
Yi Yang https://orcid.org/0000-0002-6535-8500
Danfeng Xiang https://orcid.org/0000-0002-1089-1519
Xiaofeng Wang https://orcid.org/0000-0002-7334-2357
Bo Wang https://orcid.org/0000-0002-3231-1167

References

Blinnikov, S. 2017, in Handbook of Supernovae, ed. A. W. Alsabti & P. Murdin (Berlin: Springer), 843
Blinnikov, S., Lundqvist, P., Bartunov, O., Nomoto, K., & Iwamoto, K. 2000, ApJ, 532, 1132
Blinnikov, S. I., & Bartunov, O. S. 1993, A&A, 273, 106
Blinnikov, S. I., Eastman, R., Bartunov, O. S., Popolitov, V. A., & Woosley, S. E. 1998, ApJ, 496, 454
Blinnikov, S. I., & Panov, I. V. 1996, AstL, 22, 39
Blinnikov, S. I., Röpke, F. K., Sorokina, E. I., et al. 2006, A&A, 453, 229
Blinnikov, S. I., & Tolstov, A. G. 2011, AstL, 37, 194
Dan, M., Rosswog, S., Brüggen, M., & Podsiadlowski, P. 2014, MNRAS, 438, 14
Davis, K. W., Taggart, K., Tinyanont, S., et al. 2023, MNRAS, 523, 2530
Dessart, L., Burrows, A., Ott, C. D., et al. 2006, ApJ, 644, 1063
Filippenko, A. V. 1997, ARA&A, 35, 309
Fraser, M., Stritzinger, M. D., Brennan, S. J., et al. 2021, arXiv:2108.07278
Gal-Yam, A. 2017, in Handbook of Supernovae, ed. A. W. Alsabti & P. Murdin (Berlin: Springer), 195
Gal-Yam, A., Bruch, R., Schulze, S., et al. 2022, Natur, 601, 201
Kitaura, F. S., Janka, H. T., & Hillebrandt, W. 2006, A&A, 450, 345
Kleiser, I. K. W., & Kasen, D. 2014, MNRAS, 438, 318
Kurucz, R. L., & Bell, B. 1995, Atomic line list (Cambridge, MA: Smithsonian Astrophysical Observatory)
Moriya, T. J., & Eldridge, J. J. 2016, MNRAS, 461, 2155
Moriya, T. J., Suzuki, A., Takiwaki, T., Pan, Y.-C., & Blinnikov, S. I. 2020, MNRAS, 497, 1619
Nagao, T., Kuncarayakti, H., Maeda, K., et al. 2023, A&A, 673, A27
Paxton, B., Bildsten, L., Dotter, A., et al. 2011, ApJS, 192, 3
Paxton, B., Cantiello, M., Arras, P., et al. 2013, ApJS, 208, 4
Paxton, B., Marchant, P., Schwab, J., et al. 2015, ApJS, 220, 15
Paxton, B., Schwab, J., Bauer, E. B., et al. 2018, ApJS, 234, 34
Paxton, B., Smolec, R., Schwab, J., et al. 2019, ApJS, 243, 10
Pellegrino, C., Howell, D. A., Terreran, G., et al. 2022, ApJ, 938, 73
Perley, D. A., Sollerman, J., Schulze, S., et al. 2022, ApJ, 927, 180
Schwab, J. 2021, ApJ, 906, 53
Smith, N. 2017, in Handbook of Supernovae, ed. A. W. Alsabti & P. Murdin (Berlin: Springer), 403
Tauris, T. M., Langer, N., Moriya, T. J., et al. 2013, ApJL, 778, L23
Tauris, T. M., Langer, N., & Podsiadlowski, P. 2015, MNRAS, 451, 2123
Verner, D. A., Verner, E. M., & Ferland, G. J. 1996, ADNDT, 64, 1
Wu, C., Xiong, H., Lin, J., et al. 2023, ApJL, 944, L54
Zha, S., O'Connor, E. P., Couch, S. M., Leung, S.-C., & Nomoto, K. 2022, MNRAS, 513, 1317